Increased temperature acceptance bandwidth in frequency-doubling process using two different crystals

Lulu Wang (王路露)[1,2], Ying Chen (陈 英)[1,2*], and Guangcan Liu (刘光灿)[2]

[1]Key Laboratory for Micro-/Nano-Optoelectronic Devices of Ministry of Education, College of Physics and Microelectronic Science, Hunan University, Changsha 410082, China

[2]Department of Electronic and Communication, Changsha University, Changsha 410003, China

[*]Corresponding author: yingchen@hnu.edu.cn

Received June 10, 2014; accepted August 8, 2014; posted online October 24, 2014

The temperature acceptance bandwidth of second-harmonic generation (SHG) can be dramatically improved by using two different kinds of nonlinear crystals with opposite signs of temperature derivation of phase mismatch. We study two SHG processes for the existing 1064 and 1550 nm high-average-power lasers. The numerical results show that the temperature acceptance bandwidth for SHG at 1064 nm can be three to five times larger than that of traditional single-crystal design, and it is also larger than that of using temperature-insensitive yttrium calcium oxyborate crystal. Importantly, the proposed design is applicable to various wavelengths, which suggests its potential in high-average-power SHG applications.

OCIS codes: 140.3515, 190.4223,;190.2620.

doi: 10.3788/COL201412.111902.

Two-crystal or multicrystal design has been widely used in frequency conversion process. For continuous-wave laser radiations, a cascaded multicrystal scheme can provide a single-pass doubling efficiency as high as 65% at any given fundamental power[1,2]. For femtosecond short pulses, a multicrystal design was used for compensating the spatial or temporal walk-off in the frequency conversion process. As a result, the conversion efficiency has substantially improved relative to single-crystal design[3]. Two-crystal design with orthogonal walk-off planes was also used in parametric amplification and oscillation processes for improving the conversion efficiency and beam quality of signal wave[4]. For high-peak-power lasers with a low repetition rate, a broader conversion bandwidth is favored both in inertial–confinement fusion experiments and in laser itself. First, a dual-tripler scheme design was adopted in the OMEGA laser system, and a threefold increase in bandwidth of third-harmonic generation was demonstrated in the experiment[5]. In Shen Guang II laser system, the acceptance bandwidth of second-harmonic generation (SHG) was close to 10 nm by using two type-II KH_2PO_4 (KDP) crystals, and the doubling efficiency reached 70% for top-hat chirp pulse in theory[6]. For high-average-power lasers, however, the thermal effect can result in limited conversion efficiency and unsatisfied beam quality due to the thermal-induced phase mismatch. At present, average powers over 10 kW or even 100 kW can be generated directly from the diode-pumped solid-state lasers, while the maximum output power of SHG of only ~700 W (doubling efficiency ~35%) has been demonstrated from a Q-switched Yb:YAG thin-disc laser[7,8].

Since 1980, several methods have been used to control the thermal effect in high-average-power SHG processes, such as electro-optic compensation, piezo-optic tuning, and beam shaping[9,10]. However, these techniques need extra sophisticated components, which make the operation inconvenient. Furthermore, the harmonic power did not increase significantly by using these methods. On the other hand, attempts are made to seek unique nonlinear crystals which have temperature-insensitive phase-matching (PM) properties. However, this temperature-insensitive scheme can be realized only at a specific wavelength for a certain crystal, such as yttrium calcium oxyborate (YCOB) and deuterated l-arginine phosphate for type-I SHG at fundamental wavelength of 1064 nm[11-13] and $RbTiOPO_4$ for type-II SHG at fundamental wavelength of 1030 nm[14].

Here we apply the two-crystal design to compensate for the phase mismatch in SHG process of high-average-power laser. Unlike the previous two-crystal design using identical nonlinear crystals, our proposed scheme involves two different crystals. These two crystals have opposite signs of the first derivation of phase mismatches to temperature ($\partial\Delta k/\partial T$). The phase mismatch $\Delta k(T)$ is defined as $\Delta k = k_{SH} - 2k_{FH}$, where FH and SH denote fundamental and second-harmonic waves, respectively. In this letter, we present such a design for two typical SHG cases at fundamental wavelengths of ~1 and 1.5 mm, corresponding to two currently available wavelengths of high-average-power laser.

For high-average-power lasers, the phase mismatch is mainly caused due to the non-uniform thermal effect in nonlinear crystals. If the signs of thermal-induced phase mismatch are opposite in the two cascading crystals, the phase mismatch accumulated in the first crystal can be well compensated for in the second one. So the main objective of our proposed two-crystal design in this letter

is to find out two types of nonlinear crystals which have opposite signs of $\partial\Delta k/\partial T$. The dependence of $\partial\Delta k/\partial T$ on FH wavelength is shown in Fig. 1 for four typical nonlinear crystals, that is, KDP, LiB_3O_5 (LBO), BaB_2O_4 (BBO), and YCOB. Here all the data are calculated by using the Sellmeier equations with the parameters in SNLO version 21[15], and the initial temperature is fixed at 20 °C. As shown by the squares in Fig. 1, the sign of $\partial\Delta k/\partial T$ is negative for LBO at a wide range of wavelengths (from ~700 nm to over 1.15 mm). Also the sign of $\partial\Delta k/\partial T$ in YCOB crystal is also in negative range from the wavelength of ~900 nm to over 2 mm (triangle and solid line). The signs of $\partial\Delta k/\partial T$ are always positive for KDP and BBO crystals in the transmission range (circle and dashed line). Therefore, it is always possible to find two types of crystals with opposite signs of $\partial\Delta k/\partial T$ within a broad range of wavelength (from ~700 nm to over 2 mm). Furthermore, $\partial\Delta k/\partial T$ may reach zero at a specific wavelength of ~1100 nm for YCOB in the xz plane[11], namely, YCOB crystal has the characteristics of temperature-insensitive PM in the xz plane.

For type-I SHG of a high-average-power laser, the temporal effect is negligible (i.e., assuming the pulse width much longer than 1 ps), it is considered by taking thermal-induced $\Delta k(T)$ into account. The nonlinear coupled-wave equations are used to simulate this SHG process. The equations that govern the envelopes $E_1(z)$ and $E_2(z)$ of the FH and SH waves[16], respectively, are

$$\begin{cases} \dfrac{\partial E_1(z)}{\partial z} = \mathrm{i}\dfrac{\omega_1^{\,2} d_{\mathrm{eff}}}{c^2 k_1} E_1^{\,*}(z) E_2(z) \exp\{-\mathrm{i}\Delta k(T) z\}, \\ \dfrac{\partial E_2(z)}{\partial z} = \mathrm{i}\dfrac{\omega_2^{\,2} d_{\mathrm{eff}}}{2c^2 k_2} E_1^{\,2}(z) \exp\{\mathrm{i}\Delta k(T) z\}, \end{cases} \tag{1}$$

where ω_i $(i = 1, 2)$ is the central frequency of FH $(i = 1)$ or SH $(i = 2)$ waves, respectively, and d_{eff} is the effective nonlinear coefficient. In general, the temperature acceptance bandwidth is defined as a measure for the sensitivity of conversion efficiency to temperature deviation[17]. We will numerically calculate the temperature acceptance bandwidth of SHG at two typical wavelengths of 1064 and 1550 nm, respectively.

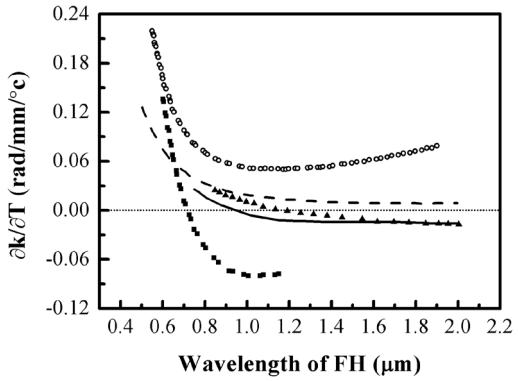

Fig. 1. $\partial\Delta k/\partial T$ as a function of FH wavelength. Circle, KDP crystal; dashed line, BBO crystal; triangle, YCOB in the xz plane; solid line, YCOB in the xy plane; square, LBO in the xy plane.

Firstly, type-I SHG process for 1064 nm laser is studied within a temperature-variation range from 20 to 60 °C (Fig. 2). In the calculations, we globally change the temperature of crystal to simulate thermal-induced temperature variations. For our proposed two-crystal design, the YCOB in the xy plane cascading with BBO crystal are chosen. We compare our results with the results obtained using a single-crystal design, that is, YCOB in the xy plane, BBO, and temperature-insensitive YCOB in the xz plane. For a fair comparison, these crystal lengths of all designs are set up with a same SHG efficiency at the initial PM temperature of 20 °C. To be specific, the lengths of single-crystal design for YCOB in the xy plane, BBO, and YCOB in the xz plane are 53, 9, and 20 mm, respectively. The lengths of YCOB in the xy plane and BBO for our two-crystal design are 16 and 6 mm, respectively. As shown in Fig. 2, the larger the deviation of initial temperature the lower the SHG efficiency. As a matter of fact, more temperature deviations mean larger thermal effect-induced phase mismatches, resulting in lower SHG efficiency. Under small-signal regime, traditional single-crystal design is quite sensitive to temperature variation (circle and triangle in Fig. 2(a)). The temperature acceptance bandwidth, defined by the full-width at half maximum (FWHM), is only ~16 °C for YCOB in the xy plane and ~38 °C for BBO. By using the two-crystal design (solid line), the temperature acceptance bandwidth can be as large as ~60 °C, which is close to the result of temperature-insensitive YCOB in the xz plane (~72 °C, dashed line). It clearly demonstrates that our proposed design can substantially reduce the sensitivity of SHG efficiency to temperature variation. Moreover, if three crystals (i.e., 3.5 mm long BBO, 10 mm long YCOB in the xy plane, and 3.5 mm long BBO in sequence) are adopted in our proposed design, the SHG efficiency can be much more insensitive to crystal temperature variation (temperature acceptance bandwidth ~100 °C, square).

SHG processes are also studied under high-efficiency regime, as shown in Fig. 2(b). The intensity of incident FH wave is assumed to be 0.2 GW/cm^2, and other parameters are similar to those in Fig. 2(a). Figure 2(b) shows that the temperature acceptance bandwidth of two-crystal design (~70 °C, solid line) is ~5 times larger than that of using single YCOB crystal in the xy plane (~14 °C, circle). And it is also larger than that of using temperature-insensitive YCOB crystal in the xz plane (dashed line). Moreover, it can be seen that the temperature acceptance bandwidth of all single-crystal designs in high-efficiency regime is smaller than that in small-signal regime by comparing with Fig. 2. Taking a single temperature-insensitive YCOB crystal as an example (dashed line in Fig. 2), the acceptance bandwidth is reduced from ~72 °C under small-signal

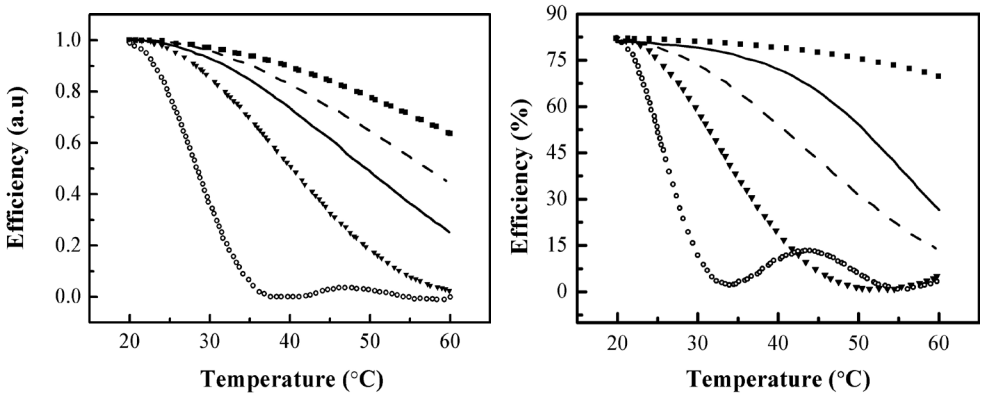

Fig. 2. Calculated type-I SHG efficiency at 1064 nm versus the crystal temperature. Square, the three-crystal design; dashed line, temperature-insensitive YCOB in the *xz* plane; solid line, the two-crystal design; triangle and circle, traditional single BBO and YCOB in the *xy* plane, respectively. The lengths of all crystals are listed above. (a) Under small-signal regime. All efficiencies are normalized to the maximal value. (b) Under high-efficiency regime with pump intensity of 0.2 GW/cm^2.

regime to only ~52 °C under high-efficiency regime. The situation in the two-crystal design, however, will be very different. The temperature acceptance bandwidth does not decrease but increase from ~60 °C under small-signal regime to ~70 °C under high-efficiency regime. This is a unique feature of our proposed two-crystal design, which suggests its potential in practical high-average-power SHG applications. Moreover, the temperature acceptance bandwidth for the three-crystal design can be increased to ~130 °C.

The transverse distribution of crystal temperature cannot be considered in all the above discussions, and are discussed below. It is known that the radial temperature profile exhibited a quadratic behavior within the pump region under the conventional edge cooling[18]. Here we employ a quadratic temperature distribution function of crystal $T(r)$ by fitting the maximum and the minimum temperatures of crystal, which can be described as

$$T(r) = T_{\max} - \frac{T_{\max} - T_{\min}}{w_0^2} r^2 (r \le w_0), \tag{2}$$

where w_0 is the radius of the laser beam, $T_{\max}$ is the maximum temperature at the crystal axis (the beam center), and $T_{\min}$ is the minimum temperature on the crystal edge (the beam edge).

The beam profiles of output SHG for single-crystal and multicrystal designs are shown in Fig. 3. In this letter, a flat-top fundamental beam with a diameter of 20 mm is adopted, the maximum temperature at the crystal axis is 50 °C and the minimum on the beam edge is 20 °C. In order to achieve a high SHG efficiency, the temperature satisfying initial PM condition should be set at 35 °C (i.e., the mid-point between 50 and 20 °C). The other parameters are the same as those used in Fig. 2. It is clearly demonstrated that the SHG efficiency for single-crystal design reduces greatly in the case of transverse distribution of crystal temperature (dashed line, triangle, and circle in Fig. 3). The beam profile of output SH even degenerates into a ring-like shape in the worst case (circle, YCOB crystal in the *xy* plane). The situation in the two-crystal design, however, is not the same. It not only supports a high SHG efficiency but also maintains a uniform SH beam profile (solid line), which is of great concern to high-power laser.

Most of all, the temperature-insensitive characteristic of our proposed design is independent of FH wavelength. As an example, the type-I SHG process of other existing high-average-power laser with the wavelength of 1550 nm is considered next. Note that there are no temperature-insensitive crystals available at this wavelength so far. For the two-crystal design, a combination of YCOB and BBO can also be a good choice, as shown in Fig. 1. The effective nonlinear coefficient of YCOB crystal in the *xz* plane is ~5 times larger than that in the *xy* plane for type-I SHG at 1550 nm[15]. Therefore,

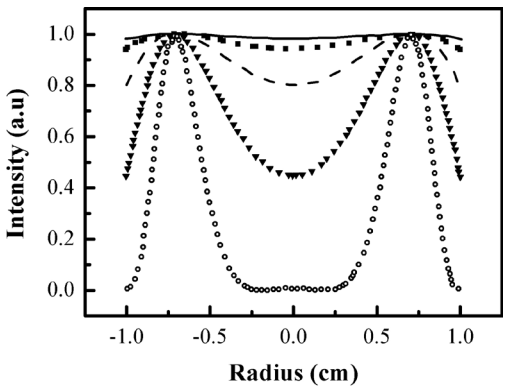

Fig. 3. Calculated beam profiles of output SHG fields. Solid line, the two-crystal design; square, the three-crystal design; dashed line, YCOB in the *xz* plane; triangle, BBO; circle, YCOB in the *xy* plane. The lengths of all crystals are the same as that in Fig. 2. The corresponding SHG efficiencies from top to bottom are 80%, 78%, 73%, 60%, and 25%, respectively.

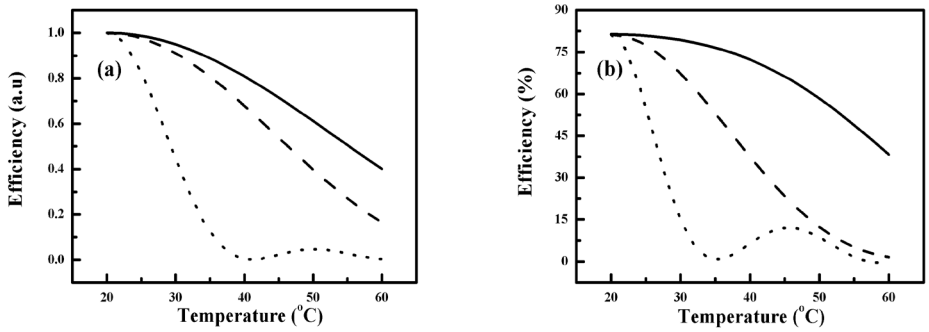

(a) (b)

Fig. 4. Calculated SHG efficiency at 1550 nm versus the crystal temperature. Solid line, 6 mm long YCOB in the *xz* plane and 10 mm long BBO; dashed line, 13 mm long BBO; dotted line, 26 mm long YCOB in the *xz* plane. (a) Under small-signal regime. (b) Under high-efficiency regime with pump intensity of 0.2 GW/cm^2.

we take YCOB crystal in the *xz* plane as the one with negative $\partial\Delta k/\partial T$. Figure 4 shows the SHG efficiency as a function of crystal temperature variations, which is calculated by using the same assumption and input FH intensity as that in Fig. 2. Similar to the case of SHG at 1064 nm, the two-crystal design also exhibits a greatly promoted insensitivity to temperature variation relative to single-crystal designs. For instance, the temperature acceptance bandwidths are only ~14 °C for YCOB in the *xy* plane and ~36 °C for BBO under high-efficiency regime (see dotted and dashed lines in Fig. 4(b)). However, the temperature acceptance bandwidth can be as large as ~75 °C by using the two-crystal design (solid line).

In conclusion, we propose the two-crystal design which can be applied to improve the temperature acceptance bandwidth of SHG process for high-average power laser. By employing two different kinds of nonlinear crystals with opposite signs of $\partial\Delta k/\partial T$, the phase mismatch accumulated in the first crystal can be compensated for in the cascading one. Thus the temperature acceptance bandwidth improves substantially. We present two typical SHG examples at wavelengths of ~1 and 1.5 μm. Numerical simulations show that the temperature acceptance bandwidth can be three to five times larger than that of traditional single-crystal designs under high-efficiency regime. Importantly, the temperature-insensitive characteristic of our proposed two-crystal design is independent of FH wavelength, which provides a promising route to generate harmonic wave of high average power at various wavelengths.

This work was partially supported by the National Natural Science Foundation of China (No. 61308005), the China Postdoctoral Science Foundation Funded Project (No. 2013M542106), the Hunan Postdoctoral Scientific Program (No. 2013RS4047), the Scientific Research Fund of Hunan Provincial Education Department (No. 14C0099), and the Science and Technology Program of Changsha (No. K1309012-11).

References

1. G. K. Samanta, S. C. Kumar, K. Devi, and M. Ebrahim-Zadeh, Opt. Lett. **35,** 3513 (2010).
2. S. Zhang, L. Guo, M. Li, L. Zhang, X. Yan, W. Hou, X. Lin, and J. Li, Chin. Opt. Lett. **10,** 071401 (2012).
3. A. V. Smith, D. J. Armstrong, and W. J. Alford, J. Opt. Soc. Am. B **15,** 122 (1998).
4. Ø. Farsund, G. Arisholm, and G. Rustad, Opt. Express **18,** 9229 (2010).
5. A. Babushkin, R. S. Craxton, S. Oskoui, M. J. Guardalben, R. L. Keck, and W. Seka, Opt. Lett. **23,** 927 (1998).
6. L. Ji, B. Zhu, C. Liu, T. Wang, and Z. Lin, Chin. Opt. Lett. **12,** 031902 (2014).
7. C. Stolzenburg, W. Schule, I. Zawischa, A. Killi, and D. Sutteret, Proc. SPIE **7578,** 75780A (2010).
8. S. Liu, L. Dong, B. Zhang, J. He, Z. Wang, J. Ning, R. Wang, and X. Liu, Chin. Opt. Lett. **12,** 031402 (2014).
9. D. Cao, X. Zhang, W. Zheng, S. He, and Z. Sui, Chin. Opt. Lett. **5,** 292 (2007).
10. D. Hon and D. H. Bruesselbach, IEEE J. Quant. Electron. **16,** 1356 (1980).
11. N. Umemura, M. Ando, K. Suzuki, E. Takaoka, K. Kato, M. Yoshimura, Y. Mori, and T. Sasaki, Jpn. J. Appl. Phys. **42,** 5040 (2003).
12. M. Sun, L. Ji, Q. Bi, N. Wang, J. Kang, X. Xie, and Z. Lin, Chin. Opt. Lett. **9,** 101901 (2011).
13. C. E. Barker, D. Eimerl, and S. P. Velsko, J. Opt. Soc. Am. B **8,** 2481 (1991).
14. L. Deyra, X. Délen, G. Mennerat, P. Villeval, F. Balembois, and P. Georges, *in Advanced Solid-State Lasers Congress* AM4A.39 (2013).
15. A.V. Smith, *SNLO Nonlinear Optics Code* (Sandia National Laboratories, Albuquerque, 2012).
16. D. Eimerl, IEEE J. Quant. Electron. **23,** 575 (1987).
17. M. Webb, IEEE J. Quant. Electron. **30,** 1934 (1994).
18. Y. F. Chen, T. M. Huang, C. F. Kao, C. L. Wang, and S. C. Wang, IEEE J. Quant. Electron. **33,** 1424 (1997).